Neutrally stable transition of a curved-crease planar shell structure

Kok, Sjaak; Radaelli, Giuseppe; Amoozandeh Nobaveh, Ali; Herder, Just

DOI
10.1016/j.eml.2021.101469

Publication date
2021

Document Version
Final published version

Published in
Extreme Mechanics Letters

Extreme Mechanics Letters 49 (2021) 101469

Contents lists available at ScienceDirect

Extreme Mechanics Letters

journal homepage: www.elsevier.com/locate/eml

Neutrally stable transition of a curved-crease planar shell structure

Sjaak Kok, Giuseppe Radaelli *, Ali Amoozandeh Nobaveh, Just Herder

Dept. Precision and Microsystems Engineering, Delft University of Technology, Delft, 2628 CD, The Netherlands

ARTICLE INFO

Article history:
Received 17 June 2021
Received in revised form 6 July 2021
Accepted 12 August 2021
Available online 25 August 2021

Keywords:
Compliant shell mechanisms
Neutral stability
Zero stiffness
Curved creases
Origami
Multi-stability

ABSTRACT

Elastic neutral stability in compliant mechanisms is a remarkable appearance since it requires the energetic state of the structure to remain unchanged during a deformation mode. Several examples in literature require either plastic deformation or external constraints to be enforced to obtain a state of pre-stress and often require the use of anisotropic materials. This paper presents a new type of compliant shell structure featuring a neutrally stable deformation mode without requiring one of the aforementioned conditions. The shell structure is composed of two initially flat compliant facets that are connected via a curved crease. The structure can be reconfigured into a second zero-energy state via propagation of a transition region, without any apparent effort. Both the structure's local width and local crease curvature can be tuned to reach neutral stability during transition. The modelled results are verified by several prototypes that match the modelled predictions qualitatively, as well as by measurement results that show quantitative agreement. The new type of structure introduced here features neutral stability without relying on the application of pre-stress during manufacturing or externally applied boundary conditions. Moreover, it shows potential for combining geometric simplicity with complex and highly tune-able behaviour.

1. Introduction

A surprisingly simple yet intriguing structure arises when two flat arched-shaped compliant sheets are stacked and connected in a hinged fashion along their shortest curved edges. The resulting mechanism features two obvious stable zero-energy equilibrium configurations: as-fabricated and inverted, with either the top sides or the bottom sides of the arches facing each other. However, *transition* between the stable states is not straightforward since the curved nature of the hinge does not allow energy-free operation. This type of hinge can be considered a curved crease and, therefore, the structure can be classified as curved-crease origami. In this type of structure, actuation of the curved crease is inherently coupled to deformation of the facets [1]. The structure can then arguably be classified as a compliant facet origami mechanism (COFOM), an origami mechanism wherein compliance of the facets is used to incorporate energy storage [2].

The transition is initiated when the edges at an arbitrary end are flipped with respect to each other (Fig. 1). As the *transition region* is propagated through, it progressively inverts the structure until it has been completely flipped over. A significant part in middle stage of this transition appears to be an energy-free process since the transition region merely shifts through the structure. The mechanism then features a continuous equilibrium as its behaviour resembles the fascinating class of statically balanced structures. In that particular situation, it is said to be 'neutrally stable'.

Elastic neutral stability is a remarkable appearance since, normally, the deformation of materials is associated with increasing potential energy and a resulting opposing force or moment. An elastic mechanism in neutral equilibrium can only deform without load if the necessary energy for deformation is already stored in the system and redistributed upon reconfiguration [3]. This unique property is investigated by Guest et al. [4], who utilize plastic deformation of an initially flat rectangular plate as a source for pre-stress and describe the behaviour of the resulting neutrally stable cylindrically curved shell. Because of residual stresses, rotation of the axis of curvature does not change the strain energy, thereby rendering all possible curvature-axes configurations equally preferable. Schultz et al. [5] describe a neutrally stable deployable composite boom that is stable in both the coiled and extended state and every configuration in between.

Elastic neutral stability was probably first mentioned by Thomson and Tait [6] in the book 'Treatise on natural philosophy' (published in 1867). There, an initially straight rod is described that exhibits a state of neutral stability when the ends are connected to form a circular, pre-stressed, geometry. Rotation around its centroidal axis can occur without the need to introduce a load or to add extra energy to the system. The tape loop, first thoroughly investigated by Vehar et al. [7], is a more recent example

* Corresponding author.
E-mail address: g.radaelli@tudelft.nl (G. Radaelli).

https://doi.org/10.1016/j.eml.2021.101469

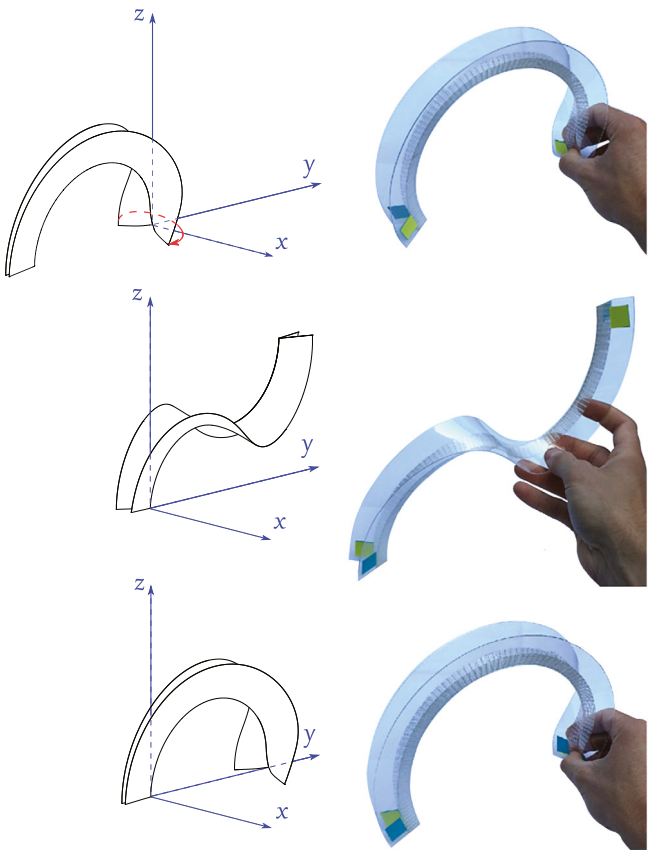

Fig. 1. The transition between the two stable zero-energy states is depicted both schematic (left) and using a physical prototype (right). After the transition is initiated (top), the transition region propagates through the structure (middle) until it reaches the opposite end (bottom).

where boundary conditions applied to a compliant shell structure result in a neutrally stable deformation mode. When the two ends of a tape spring are connected into a loop, the equilibrium configuration associated with minimal potential energy consists of two localized folds and two straight segments in-between. However, given the invariant cross-sectional geometry, the location of these folds is arbitrary, enabling these fields of energy to move through the structure without energetic costs. Given the moving regions of localized energy storage, the structure presented here closely resembles the tape loop. However, a notable difference is that no loop formation is required, resulting in an open-ended structure with beam-like properties.

Until now, all neutrally stable shell structures described in literature require either plastic deformation [4,8–11], the use of anisotropic materials [5,12–14] or external constraints to be enforced on the structure (e.g. form a loop) [6,7,15] to create the desired state of pre-stress. A fourth and unique example is given by Baumann et al. [16], where a temperature gradient causes spaghetti-shaped structures to obtain and even drive their pre-stressed neutrally stable configuration. The first two methods, might result in a complex and sensitive manufacturing process and the latter two would limit design freedom by requiring environmental conditions, thereby narrowing down the potential applications.

In this study, we present a structure that requires neither of the aforementioned conditions. In order to be the first example to fit this new class of neutrally stable structures, its neutrally stable properties need to be verified. Therefore, this study aims to characterize the unique energy-free deformation mode of this structure by examining the influence of the design parameters on its stability.

The method section of this paper addresses the approach taken to investigate the behaviour during transition, as well as the influence of two design parameters hereon. The setup of the numerical model is discussed, together with a unique choice for controlling the state of transition by manipulating the geometry of the transition region locally. The results of the numerical analysis are presented in the results section and illustrated by physical realization of several variants of the mechanism that show different behaviour. The results are quantitatively validated by measurements taken in a dedicated experimental setup. All findings are further discussed in the subsequent discussion and conclusion.

2. Mechanics of transition

The stability of the mechanism can be determined by the potential energy stored in the form of material strain. In other words, the energetic state during propagation of the transition region is a measure for the stability and existence of equilibria throughout the deformation path. The location of the transition region can be described by the location of the *inflection point* along the crease line, where the curvature of the crease line changes sign. The *inflection axis* is the material axis perpendicular to the crease line at the inflection point (Fig. 2). It is the exact location within the transition region that tends to neither of the flat equilibrium configurations and material is therefore assumed to be undeformed.

The structure consists of two identical sandwiched shells that, when assumed to be inextensible, are only subjected to bending [17]. Each can be considered a *developable ruled surface*, i.e., the mid-plane resembles a ruled surface with zero Gaussian curvature, where the local bending axes form the so-called *generators* (Fig. 2). It means that for every allowable deformation, everywhere on the surface a straight line can be traced that goes from the inner perimeter to the outer perimeter, i.e. the generators. As a consequence, everywhere on the surface one of the two principal curvatures equals zero, thus the local curvature directly relates to the bending magnitude around the local bending axis. However, it should be mentioned that the generators' directions are not invariant but are determined by the current location of the transition region. Utilizing the photoelastic effect, it can be observed that the transition region is consistently subjected to relatively high strains, suggesting that the total energy is predominantly determined by the energy stored around the inflection point (Fig. 3(a) and supplementary video 2).

The course of the energy curve during propagation of the transition region can be manipulated by design parameters of the undeformed geometry. Energy storage around the inflection point can locally be influenced by changing the amount of material (Fig. 3(b)). The local width of the arch-shaped geometry is directly proportional to the amount of material and will therefore be used as the first design variable (Fig. 4(a)). The local curvature of the crease at the location of the inflection point also influences the required material deformation (Fig. 4(b)). For instance, the limit case of a crease with zero curvature (i.e. a straight folding line) would be able to operate without deforming the material. In this work, the effect of introducing variable arch width and variable crease curvature on the behaviour of the structure during transition is further investigated.

3. Method

In order to investigate the complex geometrical configurations that occur during transition, a numerical approach is substantiated. In this section, expressions for the variable geometry are defined and modelling details are discussed.

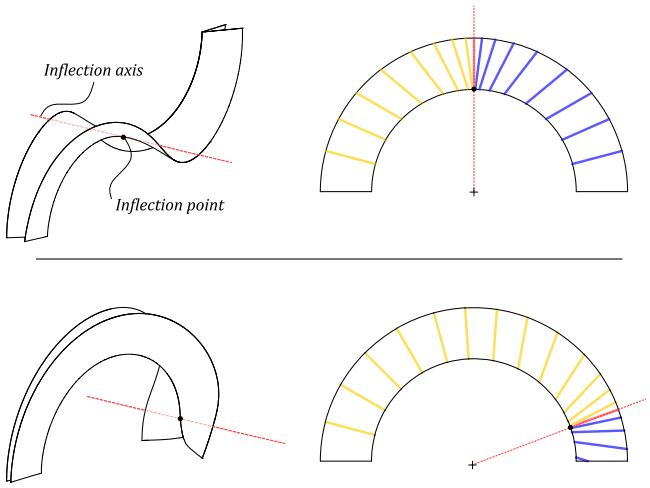

Fig. 2. The inflection point and associated inflection axis is depicted for two states during transition (left). The inflection axis is locally undeformed and directed perpendicular to the inner perimeter at the inflection point. A schematic representation of the deformation projected on the undeformed geometry is depicted (right), where the yellow and blue lines represent the generators with positive and negative curvature respectively. (For interpretation of the references to colour in this figure legend, the reader is referred to the web version of this article.)

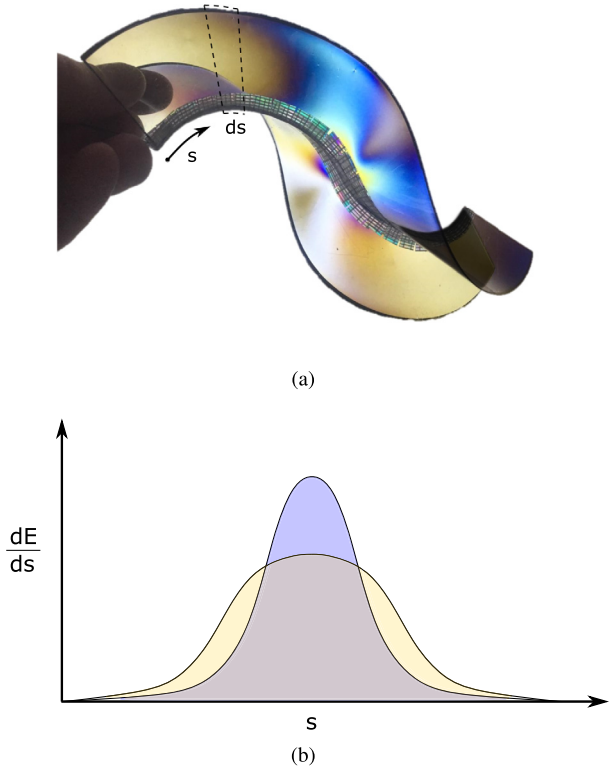

Fig. 3. (a) The stress distribution within the structure is visualized using the photoelastic effect, where colour gradients in the material represent stress gradients. (b) A schematic representation of the energy distribution as a function of the material coordinate s is also depicted. The two curves each represent a possible distribution for certain design parameters where the surface area equals the total elastic potential energy within the system. (For interpretation of the references to colour in this figure legend, the reader is referred to the web version of this article.)

3.1. Numerical model setup

An isogeometric analysis framework (IGA) [18] forms the basis of the numerical analysis. A shell model based on the Kirchhoff–Love plate theorem is used and a linear isotropic elastic constitutive law is applied. The geometry is modelled as the mid-plane surface of a shell of uniform thickness and described by B-splines. These are defined by a set of control points and make up a planar grid, with the primary and secondary material directions perpendicular to and along with the curved crease line respectively (denoted with d_1 and d_2 respectively in Fig. 5). The boundaries of the surface are given by the inner and outer perimeter, r_{in} and r_{out} respectively and a subtended angle, θ. The local width of the structure is defined as the distance between r_{in} and r_{out} perpendicular to the inner perimeter r_{in}. The control points are placed along the inner perimeter with equal angular intervals ($n = 60$) and spaced linearly along the width ($m = 10$). A Newton–Raphson numerical integration scheme is implemented in MATLAB used to solve for the static equilibrium configurations. Because of symmetry, only a single half of the structure is modelled. The effect of the interaction between the two halves is replaced with a geometrical constraint that enforces the control points that describe the crease line to live on the symmetry plane.

The effects of variations in local width and curvature are investigated separately. The local width is varied by altering the geometry of the outer perimeter while maintaining the inner perimeter constant. The addition of a sine-function of parameterized amplitude p is chosen to perturb the outer perimeter, creating a smooth transition through the structure. A parameterization of the investigated curves is given as:

$$r_{\text{w,in}}(\theta) = r_0 \tag{1}$$

$$r_{\text{w,out}}(\theta) = (1 + p \sin\theta)\, w_0 + r_0, \tag{2}$$

with

$$0 < \theta < \pi,$$

where $r_{\text{w,in}}$ describes the inner perimeter, or crease line, of constant curvature and $r_{\text{w,out}}$ describes the perturbed circular outer perimeter. r_0 is the standard radius of curvature, w_0 is the standard width (Table 1) and θ is the angular coordinate with respect to the positive x-axis. The period is chosen so that the width at the boundaries equals w_0. The amplitude p is used to produce geometries of different width profiles with $-0.4 < p < 0.4$ with equal intervals of $\Delta p = 0.1$, resulting in geometries with both narrower and wider middle sections.

An elliptical geometry is used to study the effect of local curvature. A parameterization of the investigated inner curve is given as:

$$r_{\text{c,in}}(\theta) = \frac{a_1 b_1}{\sqrt{(b_1 \cos\theta)^2 + (a_1 \sin\theta)^2}}, \tag{3}$$

with

$$a_1 = r_0$$

$$b_1 = r_0\, q$$

and

$$0 < \theta < \pi.$$

Variables a_1, b_1 are the semi-minor and semi-major axis of the inner and outer part of the perimeter respectively. The ratio between the semi-minor axis and semi-major axis is represented by the factor q, with $0.8 < q < 1.2$ with equal intervals of $\Delta q = 0.05$. A value of $q = 1$ results in a circular segment and a ratio $q > 1$ results in a geometry with higher curvature towards the boundaries. The outer perimeter $r_{\text{c,out}}$ is traced out by the last

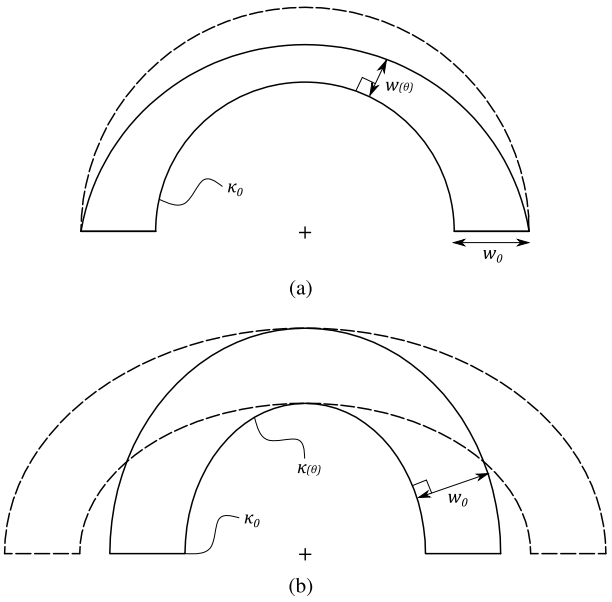

Fig. 4. A graphical representation of the design variables used to control the behaviour of the transition. Either (a) the local width is varied while maintaining a constant crease curvature or (b) the local curvature is varied while maintaining a constant width.

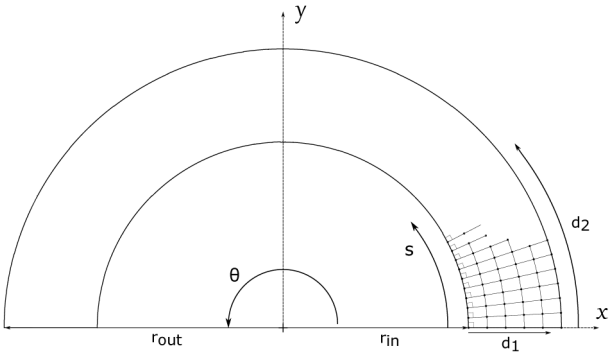

Fig. 5. The parameters used to describe the undeformed geometry are depicted in both the Cartesian and polar coordinate system. The design variables (r_{in}, r_{out}, θ), material directions used to define the control points (d_1, d_2) and the curvilinear material coordinate s are denoted.

control points in the d_1-direction, defined as the normal to the inner perimeter $r_{\text{c,in}}$ (Fig. 5). The width of the curve, measured in the direction of d_1, is kept constant and equal to w_0. Values for other design parameters are denoted in Table 1.

3.2. A moving constraint

The control points on the inner perimeter r_{in} of the modelled half of the shell structure are constrained to live on the symmetry (xy-) plane, i.e. $z = 0$. One (arbitrary) control point along r_{in} is fixed in space. The local geometry of the inflection axis can be considered as a straight line and invariant throughout the deformation process. Propagation of the transition region is therefore modelled by locally aligning the structure perpendicular to the symmetry plane (Fig. 6). The direction from control point (1) to (2) is aligned with the x-axis. Control point (3) is constrained to share its y-coordinate with point (1), such that control points (1), (2) and (3) span the xz-plane. This condition is consecutively imposed on all control points along the curved crease. The elastic potential energy during propagation is finally investigated

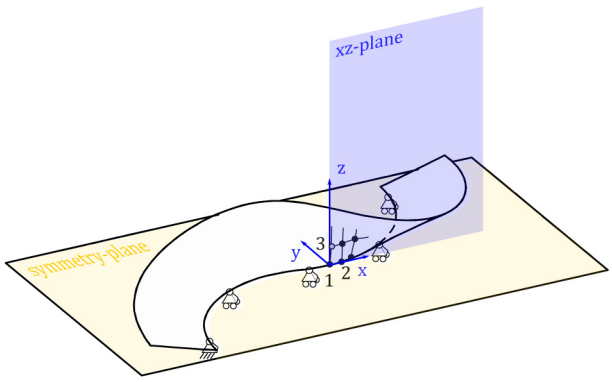

Fig. 6. The constraints used to model the propagation of the transition region. Only one half of the shell is modelled, whereby the inner perimeter r_{in} lives on the symmetry plane. Control point 1,2 and 3 are subjected to angular constraints.

Table 1
Design variables.

Parameter	Value	Unit
r_0	0.1	m
w_0	0.03	m
$\theta_{\max}$	π	rad
p	$-0.4 < p < 0.4$	–
q	$0.8 < q < 1.2$	–
t	$5e^{-4}$	m
E	$2.e^9$	$\frac{\text{N}}{\text{m}^2}$
ν	0.37	–

as a measure for the stability of all encountered intermediate configurations.

It should be noted that the resulting moving constraint affects the geometry locally, thereby omitting parasitic deformations when forces would be applied to the end point in a more generally encountered 'clamped base and end effector' loading condition.

3.3. Experimental validation

Validation of the modelled results is achieved by reproducing the constraint conditions in an experimental setup. The setup, depicted in Fig. 7, is based on a three-point bending framework that constrains three symmetrically oriented material points to be aligned over a distance d_c at a specific location along the curved crease. A 9N miniature S-beam load cell (Futek LSB200) is used together with a signal conditioner (Scaime CPJ2S) and a data acquisition module (NI USB-6008) to measure the reaction force on the middle contact point. Due to symmetry and static equilibrium conditions, the remaining two opposing reaction forces can be derived. The reaction force is a measure for the tendency of the structure to reconfigure towards an equilibrium configuration. Measurements are taken at discrete intervals of $\frac{\pi}{20}$ rad along the crease line.

Prototypes are constructed from 0.5 mm polycarbonate (PC) sheet with a Young's modulus of 2.5 GPa. Designs are modelled in CAD-CAM software and a CNC-operated drag knife is used to accurately reconstruct the modelled geometries. The curved crease is realized using glass fibre reinforced adhesive tape (3M 8959) on both sides of the PC sheets. Since a fixed distance d_c between the contact points is imposed in this setup, only geometries featuring a constant width, i.e. elliptical variations, are used for quantitative analysis. Prototypes with varying width are used to validate the modelled results qualitatively.

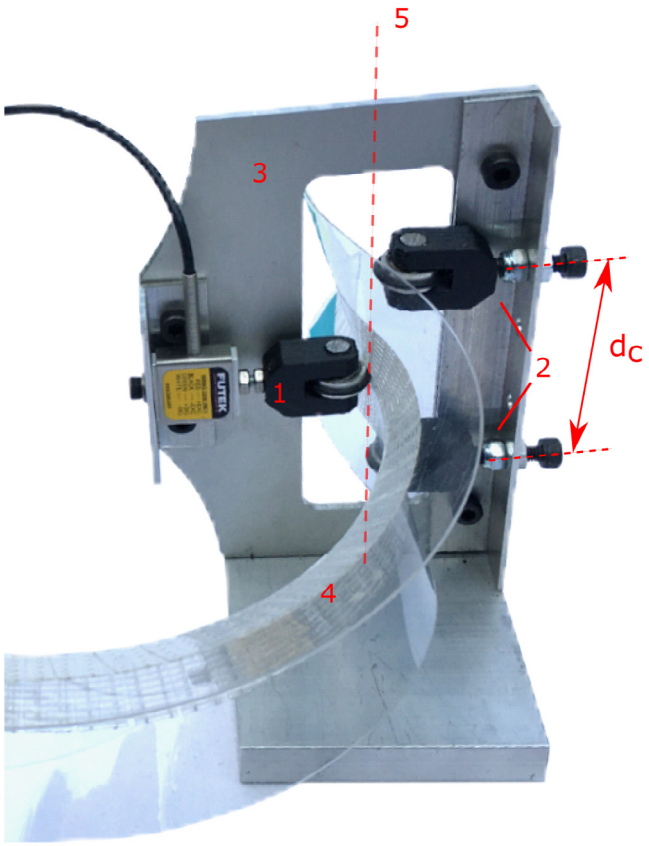

Fig. 7. The measurement setup based on a three-point bending framework. Reaction forces are measured by the middle contact point that is connected to a force transducer (1), while opposing forces are provided by two adjustable contact points (2) connected to the frame (3). Three material points are aligned on the structure to be analysed (4), representing the inflection axis (5).

4. Results

4.1. Modelling results

Figs. 8 and 9 show the elastic energy during transition of the structure with varying local width and varying local curvature respectively. Every curve represents the behaviour of a unique geometry, determined by a certain value of the parameters p and q. The dashed curve represents the same, circular, geometry with constant width in both figures. In both figures, the deformed configurations obtained from the analyses around certain locations along this dashed curve are depicted. An animated sequence of configurations during transition for $q = 1.05$ can be seen in supplementary video 1, whereby the geometry was determined by manipulation the control points around the inflection point. Note that the flat zero-energy states are not depicted here since they do not feature an inflection axis and fall therefore outside the analysis window.

4.2. Experimental results

Fig. 10 shows the reaction forces on the static contact points of four variations to the elliptical geometry. A geometry with a third equilibrium ($q = 1.2$), a constant energy region ($q = 1.05$), a circular geometry ($q = 1$) and an unstable geometry ($q = 0.9$) are investigated. The dashed lines represent the boundaries of the discrete measurement results and the markers denote the discrete measurement locations. Locations where contact was barely present are denoted with zero. The shaded area illustrates the variance in the measurement results. A change of sign of the measurement signal required a physical flip of the analysed structure to ensure continuous contact with the contact points.

Prototypes that represent the most extreme variations to the elliptical and the circular geometries have been constructed. The two variations with a predicted stable equilibrium halfway through the transition ($p = -0.4$ and $q = 1.2$) also show this behaviour in practice. Structures with a predicted unstable equilibrium ($p = 0.4$ and $q = 0.9$) always showed a tendency towards their flat configurations. Finally, prototypes with a predicted region of near-constant energy ($p = -0.1$ and $q = 1.05$) have been constructed and showed no tendency towards any configuration. Within that region, no external loads were required in order to maintain static balance. Prototypes of the elliptical extremes are depicted in Fig. 11.

5. Discussion

5.1. Results of the numerical analysis

A local energy maximum represents an unstable equilibrium, while a local energy minimum predicts the existence of a stable equilibrium. It can be seen that both geometric groups feature stable and unstable equilibria.

A circular geometry of constant width (corresponding to $p = 0$ and $q = 1$ and the dashed curves in Figs. 8 and 9 respectively) does not show stable behaviour. When the structure is symmetric with respect to the inflection point and both sides are equal in size, a local maximum exists. This effect is amplified when the middle of the structure either features higher width or higher curvature with respect to the ends (corresponding to values of $p > 0$ and $q < 1$). For values of $p < -0.05$ and $q > 1.05$, the structure exhibits a third stable, albeit non-zero-energy equilibrium. The local energy minimum implies a tendency of the mechanism to maintain this symmetric configuration. For values of p around $p = -0.05$ and $q = 1.05$, the potential elastic energy curve neither shows local maxima nor local minima around this symmetric configuration, extending the state of equilibrium over a significant portion of the investigated range of motion. This shows that compensation for the edge-effects of the open ended structure is possible, by geometrical variations to the standard circular structure of constant width. Note that this unique property is not a result of a specific optimization procedure but arises simply due to the variation of either of two principal design parameters. This aspect could be generalized by stating that the behaviour is tune-able to a high extend, creating the potential to be optimized for customized behaviour.

5.2. Results of the experimental analysis

Measurement results show similar behaviour when compared to the modelled predictions. However, measured forces are notably lower then predicted, which could be due to several discrepancies between simulations and the physical realization of the structure. The crease is modelled to have zero stiffness, while this is evidently not achievable in practice. Crease forces could have opposed the reaction forces of the shell elements, thereby affecting the measurements. Also, visco-elasticity of the prototype material was not taken into account in the numerical simulations. Moreover, the finite width of the crease allowed for some relative motion between the structure's connected edges, resulting in another mismatch with the modelled conditions. Finally, the manual operations allowed for some inconsistency regarding positioning and propagation velocity and left some room for interpretation of the measured forces. Qualitative analysis showed stable or unstable behaviour as predicted and confirmed the existence of a neutrally stable geometry in between.

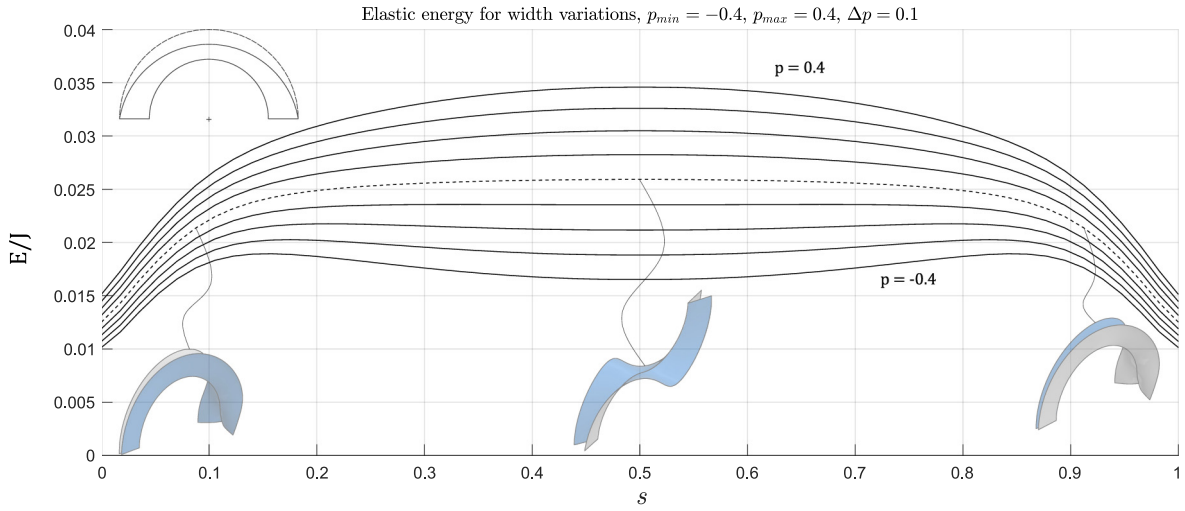

Fig. 8. The energetic paths for different values of the design parameter p, associated with a varying local width are depicted. The curves show the elastic energy during transition between the two stable zero-energy states. The dashed curve represents a structure of constant width.

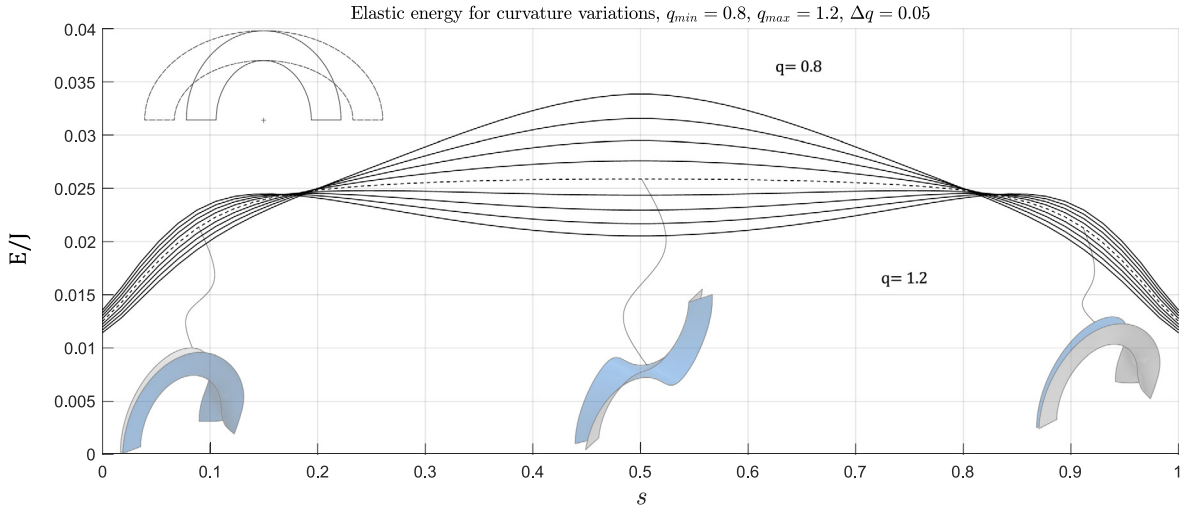

Fig. 9. The energetic paths for different values of the design parameter q, associated with a varying local curvature are depicted. The curves show the elastic energy during transition between the two stable zero-energy states. The dashed curve represents a structure of constant curvature.

5.3. Future work

The achievement of neutrally stable elastic behaviour from an structure that does not require complex pre-stress steps, opens up new opportunities in terms of embedded actuation. A passive mechanical substrate that does not absorb any elastic deformation energy, is convenient because it allows for a better input–output efficiency of the available actuation power. It is thus recommendable to explore the possibilities to apply active materials, e.g. smart memory alloys, to apply a local deformation to the structure and as such are able to move the inflection point to a desired location. The main directly observable result would be that the structure will then keep its deformed shape even when the power supply is stopped.

6. Conclusion

In this paper, a new type of neutrally stable compliant shell structure featuring a curved crease is presented. Transition between two stable zero-energy states occurs by propagating a transition region through the structure without apparent effort. This unique behaviour is characterized by analysing the influence of two principal design parameters on the stability of the encountered configurations.

It has been shown that the energetic path during transition can be manipulated by both the structure's local width and local crease curvature. For a unique set of design parameters, a third prolonged equilibrium exists within a significant range of motion, rendering the structure neutrally stable and verifying its potential to be optimized for specific behaviour. The modelled results are substantiated qualitatively by constructing several prototypes that show behaviour in agreement with the modelled predictions. Moreover, measurement results of pronounced stable and unstable geometries show quantitative agreement with the modelled results. This verifies the validity of the modelling approach.

In contrast to existing neutrally stable compliant structures, operation of the structure presented here neither requires material anisotropy, nor taylored plastic deformation nor external conditions to be enforced. Therefore, we present a new type of neutrally stable compliant structure that does not rely on the application of manufactured pre-stress or external constraints, nor on material anisotropy for operation. This type of structure allows geometric simplicity to be combined with behaviour that is generally considered complex.

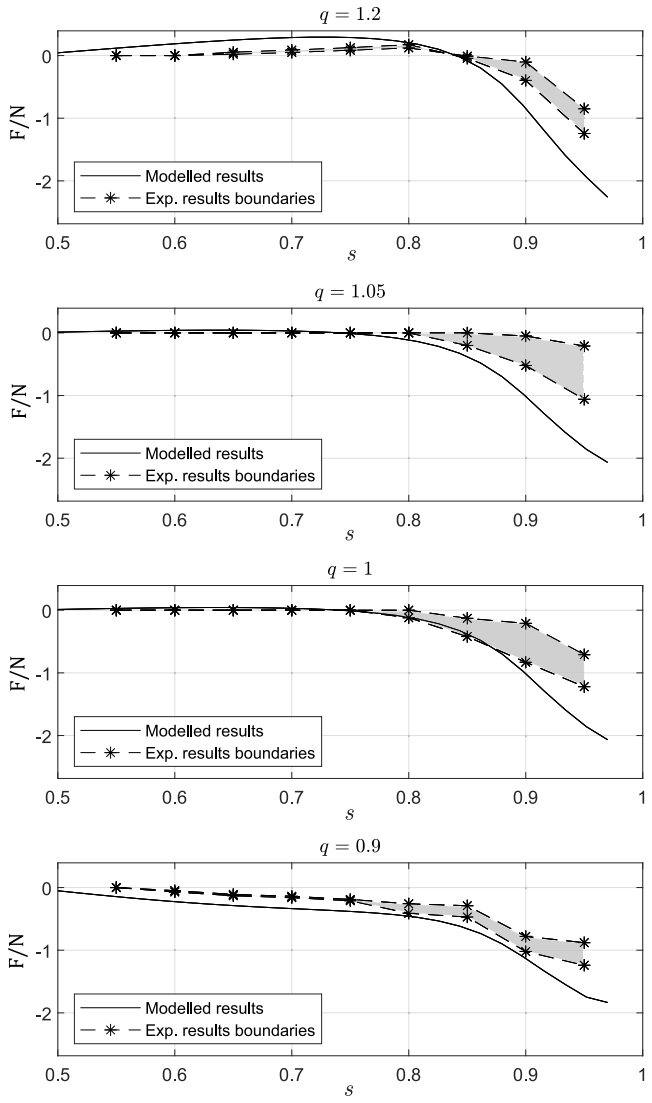

Fig. 10. The modelled and measured reaction forces depicted for an elliptic geometry for various values of the design parameter q. The solid line represents the modelled results while the dashed lines correspond to the experimental results. The shaded area depicts the spread of measurement results. The variable s on the horizontal axis describes the normalized location of the inflection point and because of symmetry. only half the transition is depicted.

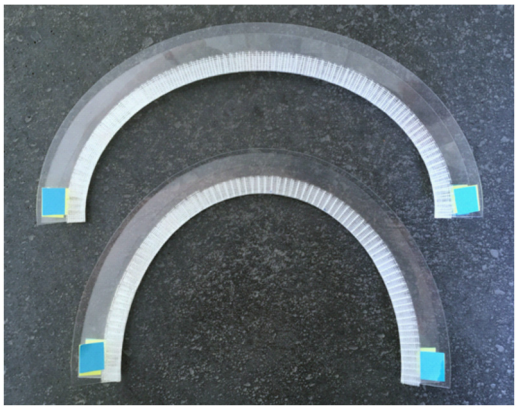

Fig. 11. Prototypes are constructed for qualitative comparison to the modelled results. Here, the two most extreme variations to the elliptical geometries, corresponding to $q = 1.2$ (top) and $q = 0.9$ (bottom) are shown.

Declaration of competing interest

The authors declare that they have no known competing financial interests or personal relationships that could have appeared to influence the work reported in this paper.

Acknowledgement

This work was supported by the Dutch Research Council (NWO), The Netherlands [P16-05 Shell-Skeletons].

Appendix A. Supplementary data

Supplementary material related to this article can be found online at https://doi.org/10.1016/j.eml.2021.101469.

References

[1] M.A. Dias, L.H. Dudte, L. Mahadevan, C.D. Santangelo, Geometric mechanics of curved crease origami, Phys. Rev. Lett. 109 (11) (2012) 1–5, http://dx.doi.org/10.1103/PhysRevLett.109.114301, arXiv:1206.0461.

[2] J. Rommers, G. Radaelli, J. Herder, A pseudo rigid body model of a single vertex compliant-facet origami mechanism (SV-COFOM), in: Proceedings of the ASME Design Engineering Technical Conference, Vol. 5B-2016, 2016, pp. 1–10, http://dx.doi.org/10.1115/DETC2016-59377.

[3] S. Kok, Towards Neutrally Stable Compliant Shells (Msc thesis), Delft University of Technology, 2020, URL http://repository.tudelft.nl/.

[4] S. Guest, E. Kebadze, S. Pellegrino, Zero stiffness elastic shell structures, Mech. Mater. Struct. 6 (1–4) (2011).

[5] M.R. Schultz, M.J. Hulse, P.N. Keller, D. Turse, Neutrally stable behavior in fiber-reinforced composite tape springs, Composites A 39 (6) (2008) 1012–1017, http://dx.doi.org/10.1016/j.compositesa.2008.03.004.

[6] W.T.B. Kelvin, P.G. Tait, Treatise on Natural Philosophy, Vol. 1, Claredon Press, 1867.

[7] C. Vehar, S. Kota, R. Dennis, Closed-loop tape springs as fully compliant mechanisms -preliminary investigations, in: Proceedings of the ASME Design Engineering Technical Conference, Vol. 2 B, 2004, pp. 1023–1032, http://dx.doi.org/10.1115/detc2004-57403.

[8] W.H. Wittrick, W.H. Wittrick, D.M. Myers, W.R. Blunden, Stability of a bimetallic disk, Q. J. Mech. Appl. Math. 6 (1) (1953) 15–31, http://dx.doi.org/10.1093/qjmam/6.1.15.

[9] E. Lamacchia, A. Pirrera, I.V. Chenchiah, P.M. Weaver, Non-axisymmetric bending of thin annular plates due to circumferentially distributed moments, Int. J. Solids Struct. 51 (3–4) (2014) 622–632, http://dx.doi.org/10.1016/j.ijsolstr.2013.10.028.

[10] K.A. Seffen, R.A. McMahon, Heating of a uniform wafer disk, Int. J. Mech. Sci. 49 (2) (2007) 230–238, http://dx.doi.org/10.1016/j.ijmecsci.2006.08.003.

[11] W. Hamouche, C. Maurini, S. Vidoli, A. Vincenti, Multi-parameter actuation of a neutrally stable shell: A flexible gear-less motor, Proc. R. Soc. A 473 (2204) (2017) http://dx.doi.org/10.1098/rspa.2017.0364, arXiv:1707.09013.

[12] J.P. Stacey, M.P. O'Donnell, M. Schenk, Thermal prestress in composite compliant shell mechanisms, J. Mech. Robot. 11 (2) (2019) 1–10, http://dx.doi.org/10.1115/1.4042476.

[13] T.W. Murphey, S. Pellegrino, A novel actuated composite tape-spring for deployable structures, in: Collection of Technical Papers - AIAA/ASME/ASCE/AHS/ASC Structures, Structural Dynamics and Materials Conference, Vol. 1, 2004, pp. 260–270, http://dx.doi.org/10.2514/6.2004-1528.

[14] Y. Liuyi, T. Huifeng, C. Zongsheng, Thin-walled neutrally stable deployable composite, 2015, pp. 19–24, (July).

[15] D.F. Wilkes, Rolamite-A new mechanical design concept, 1967.

[16] A. Baumann, A. Sánchez-Ferrer, L. Jacomine, P. Martinoty, V. Le Houerou, F. Ziebert, I.M. Kulić, Motorizing fibres with geometric zero-energy modes, Nature Mater. 17 (6) (2018) 523–527, http://dx.doi.org/10.1038/s41563-018-0062-0.

[17] E. Kebadze, S.D. Guest, S. Pellegrino, Bistable prestressed shell structures, Int. J. Solids Struct. 41 (11–12) (2004) 2801–2820, http://dx.doi.org/10.1016/j.ijsolstr.2004.01.028.

[18] A.P. Nagy, Isogeometric Design Optimisation, 2011, p. 226.